

# On the Triple Pomeron Vertex in Perturbative QCD

J.Bartels<sup>a</sup>, M.G.Ryskin<sup>b</sup>, and G.P.Vacca<sup>c</sup>

<sup>a</sup>II. Institut für Theoretische Physik; Universität Hamburg  
Luruper Chaussee 149, 22761 Hamburg, Germany <sup>1</sup>

<sup>b</sup> St.Petersburg Nuclear Physics Institute  
Gatchina, St.Petersburg 188300, Russia<sup>2</sup>

<sup>c</sup> Dipartimento di Fisica, Università di Bologna and  
Istituto Nazionale di Fisica Nucleare, Sezione di Bologna,  
via Irnerio 46, 40126 Bologna, Italy

## Abstract

We estimate the size of the triple Pomeron vertex in perturbative QCD and compare with the phenomenological value extracted from Regge fits to experimental data. For simplicity, the results of the QCD analysis are taken in the large- $N_c$  limit. We find that the perturbative triple Pomeron coupling is of the same order of magnitude as the observed one. We also estimate the size of the Pomeron self energy and its contribution to the renormalization of the Pomeron intercept. The effect is very small, in agreement with previous nonperturbative estimates.

## 1 Introduction

The Regge description of hadronic high energy scattering processes contains a few fundamental parameters which are of nonperturbative nature. Their values have been extracted from the analysis of a large variety of experimental data, and, so far, there exist no calculations within QCD which would allow a comparison of theory and experiment. Prominent examples are the Pomeron intercept  $\alpha_P(0) \approx 1.08$  and the Pomeron slope  $\alpha'_P \approx 0.25 \text{ GeV}^{-2}$ , seen in the total cross section and in elastic scattering, and the triple Pomeron coupling  $g_{3P}$ , defined and measured in high mass diffraction.

---

<sup>1</sup>Supported by the TMR Network “QCD and Deep Structure of Elementary Particles”

<sup>2</sup>Work supported by the NATO Collaborated Linkage Grant SA (PST.CLG.976453)5437 and by the RFFI grant 00-15-96610

Whereas the former two parameters refer to the (effective) Pomeron seen at present energies, it is widely believed that the latter one provides information on the origin of the Pomeron: a Pomeron with intercept exactly at one would exhibit features that are typical for systems near a phase transition point [3, 4]. In such a situation the triple Pomeron vertex which describes the splitting of a single Pomeron into two Pomerons then provides the starting point for calculating correlation functions, critical indices etc. For example, using a field theoretic description of the Pomeron, the value of the triple Pomeron coupling determines the size of the self energy, its renormalization of the intercept etc. In reality, the intercept is close to unity (but not exactly at one), so it is likely that, at present day energies, we are in the vicinity of a phase transition, and the triple Pomeron vertex plays a fundamental role.

In perturbative QCD, the Pomeron is approximated by the BFKL calculation [1] (in LO and, more recently, also in NLO [2]). However, the values for Pomeron intercept and slope are not very close to the observed hadronic values; moreover, the BFKL approximation can be justified only for scattering processes in which the scattering objects have a small transverse extension ( $\gamma^* - \gamma^*$  scattering, or onium-onium scattering). As to the Pomeron slope, for  $t \neq 0$ , the BFKL amplitude predicts a small value, whereas at  $t = 0$  the  $t$ -slope is singular, reflecting thus the long distance behavior of the perturbative massless gluons. The next parameter, the perturbative triple Pomeron vertex, has first been calculated in [5, 6], starting from the high energy behavior of QCD Feynman diagrams. Later on, independent derivations have been performed, within Feynman diagrams [7, 8], using a Wilson line approach [9] and within the QCD dipole approach [10, 11]. As far as the numerical computation of this perturbative coupling and its comparison with the experimental hadronic vertex is concerned, an important step has been done in [12, 13]: the analytic expression derived from the underlying Feynman diagrams contains conformal integrals which have been computed in [12, 13]. These results, however, do not yet allow for a direct comparison with experimental data: as it was the case already for the BFKL approximation in elastic scattering at  $t = 0$ , also the perturbative triple Pomeron vertex has a singularity at zero momentum transfer. Any numerical estimate, therefore, will depend upon the way in which this singular behavior is treated.

There is no doubt that perturbative QCD cannot be used in hadron hadron small-angle scattering. Nevertheless, the analysis of perturbation theory in this high energy limit provides the first step towards the ‘real’ theory, and it is important to see, ‘how far away from reality’ we are in pQCD. It is the purpose of this paper, to attempt a numerical estimate of the perturbative triple Pomeron vertex and to compare with the hadronic value. We start from the Feynman diagram analysis of [5, 6], and we make use of the numerical values obtained in [12, 13]. For reference we use the cross section formula for diffraction in the triple Regge region: we derive a value for the perturbative triple Pomeron vertex which can be compared to the measured hadronic value. We also estimate the self energy of the BFKL Pomeron. Some of our results differ from earlier estimates, contained in the literature [12, 14, 15].

When trying to compare BFKL predictions with the Pomeron parameters measured in hadron hadron scattering, we will face a few difficulties of general nature. First, hadron hadron scattering, to a very good approximation, has been parametrized by a simple Regge pole in the complex angular momentum plane; the leading BFKL singularity, on the other hand, is a fixed cut which leads, in addition to the Regge exponents  $s^\alpha$ , to logarithms of the energy. Furthermore, BFKL scattering amplitudes are slightly singular when the momentum transfer  $t$  is taken to zero; this singularity reflects the  $1/k^2$ -singularity of the zero mass gluon propagator in perturbative QCD. Nonperturbative effects, therefore, are expected to be particularly strong near  $t = 0$ , and a comparison between perturbative Pomeron parameters and the measured nonperturbative values looks more promising in the region of nonzero  $t$ -values.

Our paper is organized as follows. In section 2 we briefly review, for comparison, the perturbative BFKL Pomeron in elastic scattering. In section 3 we turn to the triple Regge region of diffraction and define what we mean by a ‘triple Pomeron vertex’ in perturbative QCD. Section 4 deals with the self-energy of the BFKL Pomeron. The numerical evaluation will be done in section 5. In the final section we give a summary and a few general comments. Some technical details are put into two small appendices.

## 2 Elastic scattering

In order to find the correct normalization of the triple Pomeron vertex we have to start from elastic  $2 \rightarrow 2$  scattering. Let us write down the Regge ansatz for an elastic  $2 \rightarrow 2$  scattering process. For a Pomeron pole in the complex angular momentum plane the elastic amplitude is

$$A_{el} = -e^{-i\frac{\pi}{2}\alpha(t)} g_N^2 s \left( \frac{s}{s_0} \right)^{\alpha(t)-1}, \quad (1)$$

the elastic cross section has the form

$$\frac{d\sigma}{dt} = \frac{1}{16\pi} g_N^4 \left( \frac{s}{s_0} \right)^{2\alpha(t)-2}, \quad (2)$$

and the total cross section is

$$\sigma^{\text{tot}} = g_N^2 \left( \frac{s}{s_0} \right)^{\alpha(0)-1}. \quad (3)$$

In the following we want to compare these expressions with the ones obtained from perturbative QCD in the Regge limit. In particular, we have to relate the residue functions  $g_N$  to impact factors which naturally arise in a perturbative analysis. For reasons which will become clear soon, we will have to define forward and non-forward coupling functions,  $g_F$  and  $G_{NF}$ , resp.

For a  $2 \rightarrow 2$  scattering process (e.g. gluon-gluon scattering or  $\gamma^* - \gamma^*$  scattering) a color singlet exchange leads, in lowest order  $\alpha_s$ , to the form

$$A_{el}^{\text{LO}} = i\frac{s}{2} \int \frac{d^2\mathbf{k}}{(2\pi)^3} \Phi_1(\mathbf{k}, \mathbf{q} - \mathbf{k}) \frac{1}{\mathbf{k}^2(\mathbf{q} - \mathbf{k})^2} \Phi_2(\mathbf{k}, \mathbf{q} - \mathbf{k}) \quad (4)$$

All the momenta are living in the transverse plane,  $\mathbf{q}$  (with  $t = -\mathbf{q}^2$ ) denote the momentum transfer and  $s$  the squared center of mass energy, resp, and  $\Phi_i$  is the impact factor of the scattering particle  $i$ . As an example, with this choice for the integration measure, the gluon impact factor can be written as  $g^2 2\sqrt{\pi} N_c / \sqrt{N_c^2 - 1}$ .

Summing all the contribution in the leading log  $s$  approximation leads to the BFKL Pomeron exchange; instead of the two gluon propagators we insert the BFKL Greens function. The new amplitude reads

$$A_{el}^{LL} = \frac{is}{2} \int \frac{d^2\mathbf{k}}{(2\pi)^3} \frac{d^2\mathbf{k}'}{(2\pi)^3} \Phi_1(\mathbf{k}, \mathbf{q} - \mathbf{k}) G(y|\mathbf{k}, \mathbf{q} - \mathbf{k}; \mathbf{k}', \mathbf{q} - \mathbf{k}') \Phi_2(\mathbf{k}', \mathbf{q} - \mathbf{k}'), \quad (5)$$

where  $y$  is the rapidity variable. Clearly, for  $\alpha_s \rightarrow 0$ , when all rungs of the BFKL resummation decouple, this expression reduces to the two gluon exchange, which means that we use the following normalization:

$$\lim_{\alpha_s \rightarrow 0} G(y|\mathbf{k}, \mathbf{q} - \mathbf{k}; \mathbf{k}', \mathbf{q} - \mathbf{k}') = \frac{(2\pi)^3}{\mathbf{k}^2 (\mathbf{q} - \mathbf{k})^2} \delta^{(2)}(\mathbf{k} - \mathbf{k}') \quad (6)$$



Figure 1: Elastic process

## 2.1 The BFKL Pomeron Green function

Eigenfunctions of the BFKL kernel,  $E_{h,\bar{h}}$ , are well known in coordinate space, where its form is dictated by conformal invariance

$$E_{h,\bar{h}}(\mathbf{r}_{10}, \mathbf{r}_{20}) = \left( \frac{r_{12}}{r_{10}r_{20}} \right)^h \left( \frac{r_{12}^*}{r_{10}^*r_{20}^*} \right)^{\bar{h}}, \quad (7)$$

with  $\mathbf{r}_{10} = \mathbf{r}_1 - \mathbf{r}_0$  etc,  $h = (1 + n)/2 + i\nu$ ,  $\bar{h} = (1 - n)/2 + i\nu$  ( $h^* = 1 - \bar{h}$ ,  $\bar{h}^* = 1 - h$ ), and standard complex notation for the two-dimensional vector is used on the right-hand side. Fourier transforming (we use the Lipatov's convention which assigns a  $1/(2\pi)^2$  to any coordinate integration) to momentum space one finds [16]

$$\tilde{E}_{h\bar{h}}(\mathbf{k}_1, \mathbf{k}_2) = \int \frac{d^2\mathbf{r}_1}{(2\pi)^2} \frac{d^2\mathbf{r}_2}{(2\pi)^2} E_{h,\bar{h}}(\mathbf{r}_1, \mathbf{r}_2) e^{i(\mathbf{k}_1 \cdot \mathbf{r}_1 + \mathbf{k}_2 \cdot \mathbf{r}_2)} = C(X(\mathbf{k}_1, \mathbf{k}_2) + (-1)^n X(\mathbf{k}_2, \mathbf{k}_1)). \quad (8)$$

The coefficient  $C$  is given by

$$C = \frac{(-i)^n}{(4\pi)^2} h\bar{h}(1-h)(1-\bar{h})\Gamma(1-h)\Gamma(1-\bar{h}). \quad (9)$$

The functions  $X$  in complex notation can be expressed in terms of hypergeometric functions:

$$X(\mathbf{k}_1, \mathbf{k}_2) = \left(\frac{k_1}{2}\right)^{\bar{h}-2} \left(\frac{k_2^*}{2}\right)^{h-2} F\left(1-h, 2-h; 2; -\frac{k_1^*}{k_2^*}\right) F\left(1-\bar{h}, 2-\bar{h}; 2; -\frac{k_2}{k_1}\right). \quad (10)$$

This analytic form does not contain any term of the type  $\delta^2(\mathbf{k}_1)$  or  $\delta^2(\mathbf{k}_2)$  which are present in the coordinate representation (7). For the impact factor of a colorless external particle we have the well known property, that it vanishes for zero gluon momentum: in this case the delta-function type contributions do not contribute. For simplicity, we therefore will ignore them.

The Pomeron intercept has the form  $\alpha_P(0) = 1 + \chi(\nu, n)$  where

$$\chi(\nu, n) = \bar{\alpha}_s \left( 2\psi(1) - \psi\left(\frac{1+|n|}{2} + i\nu\right) - \psi\left(\frac{1+|n|}{2} - i\nu\right) \right), \quad \bar{\alpha}_s = \frac{N_c \alpha_s}{\pi} \quad (11)$$

Let us now consider the Pomeron Green function in the coordinate representation [17]. Making use of the Casimir operator properties of the Möbius group, one can chose a representation which is more convenient to perform a Fourier Transform. In particular, after considering the relation

$$\begin{aligned} \frac{1}{|\rho_{12}|^4} E_{h,\bar{h}}(\rho_{10}, \rho_{20}) &= \frac{1}{16} |\partial_1|^2 |\partial_2|^2 \frac{1}{(\rho_{12}^2 \partial_1 \partial_2) \times (h.c.)} E_{h,\bar{h}}(\rho_{10}, \rho_{20}) \\ &= \frac{1}{16} \frac{1}{[\nu^2 + (n-1)^2/4][\nu^2 + (n+1)^2/4]} |\partial_1|^2 |\partial_2|^2 E_{h,\bar{h}}(\rho_{10}, \rho_{20}) \end{aligned} \quad (12)$$

one can write

$$G_2^{(A)}(y|\rho_1, \rho_2; \rho_{1'}, \rho_{2'}) = \int d\mu d^2\boldsymbol{\rho}_0 e^{y\chi(\nu, n)} N_h |\partial_1|^2 |\partial_2|^2 E_{h,\bar{h}}(\rho_{10}, \rho_{20}) E_{h,\bar{h}}^*(\rho_{1'0}, \rho_{2'0}) \quad (13)$$

where we use the measure in the conformal weight space  $\int d\mu = \sum_n \int d\nu$  with the following normalization factor  $N_h$ :

$$N_h = \frac{(\nu^2 + n^2/4)}{[\nu^2 + (n-1)^2/4][\nu^2 + (n+1)^2/4]}. \quad (14)$$

In order to find the momentum representation we take the Fourier transform taking into account the total momentum conservation, and we obtain:

$$\tilde{G}_2^{(A)}(y|\mathbf{k}_1, \mathbf{k}_2; \mathbf{k}_{1'}, \mathbf{k}_{2'}) = (2\pi)^3 \int d\mu e^{y\chi(\nu, n)} N_h \times (2\pi)^2 |\mathbf{k}_1|^2 |\mathbf{q} - \mathbf{k}_1|^2 \tilde{E}_{h,\bar{h}}(\mathbf{k}_1, \mathbf{q} - \mathbf{k}_1) \tilde{E}_{h,\bar{h}}^*(\mathbf{k}_{1'}, \mathbf{q} - \mathbf{k}_{1'}). \quad (15)$$

The  $(2\pi)^3$  factor in front of the integral comes from the normalization (6); the second  $(2\pi)^2$  factor results from the  $\boldsymbol{\rho}_0$  integration, together with a  $\delta^{(2)}(\mathbf{k}_1 + \mathbf{k}_2 - \mathbf{k}_{1'} - \mathbf{k}_{2'})$  related to the overall momentum conservation. As before,  $\mathbf{q} = \mathbf{k}_1 + \mathbf{k}_2 = \mathbf{k}_{1'} + \mathbf{k}_{2'}$  is the conserved exchanged momentum. This form of the Green function is amputated on the lhs, i.e. for the gluons with momenta  $\mathbf{k}_1$  and  $\mathbf{k}_2$ . Clearly, dividing by  $|\mathbf{k}_1|^2 |\mathbf{q} - \mathbf{k}_1|^2$  one arrives at the nonamputated Green's function  $\tilde{G}_2^{(NA)}$ .

## 2.2 Extraction of the couplings $g_F$ and $g_{NF}$

Substituting in (5) the expression of the BFKL Pomeron Green's function the elastic scattering amplitude can be written as:

$$A_{el}^{LL}(\mathbf{q}) = \frac{is}{2}(2\pi)^5 \sum_n \int d\nu N_h e^{y\chi(\nu,n)} \Phi_1^h(\mathbf{q})\Phi_2^{h*}(\mathbf{q}), \quad (16)$$

where

$$\Phi_i^h(\mathbf{q}) = \int \frac{d^2\mathbf{k}}{(2\pi)^3} \tilde{E}_{h,\bar{h}}(\mathbf{k}, \mathbf{q} - \mathbf{k}) \Phi_i(\mathbf{k}, \mathbf{q} - \mathbf{k}) \quad (17)$$

are the impact factors in the conformal representation, i.e. integrated with the BFKL Pomeron eigenstates, and  $\mathbf{q}$  is the total transverse momenta exchanged.

For our purposes it will be sufficient to consider the elastic scattering of identical particles. We will consider the forward ( $\mathbf{q} = 0$ ) and the non forward ( $\mathbf{q} \neq 0$ ) case separately. Since we are interested in the leading high energy behavior, we restrict ourselves to the conformal spin  $n = 0$ , and we perform the integration in  $\nu$  in the saddle point approximation for  $y \rightarrow \infty$ . We therefore need to know the behaviour of  $\Phi_i^h$  as a function of  $\nu$ . In the appendix we show that the forward ( $\Phi_F$ ) and non forward ( $\Phi_{NF}$ ) cases are different. Near the saddle point at  $\nu = 0$  we find:

$$\Phi_F = \frac{1}{i\nu} \Phi_{0F} + O(\nu^0), \quad \Phi_{NF} = \Phi_{0NF} + O(\nu), \quad (18)$$

Moreover, we have  $N_h = 16\nu^2$ . Next we need the expansion

$$\chi(\nu, 0) = \chi_0 - a\nu^2, \quad \chi_0 = 4 \ln(2)\bar{\alpha}_s \quad a = 14\zeta(3)\bar{\alpha}_s. \quad (19)$$

In the forward case  $\mathbf{q} = 0$  we obtain

$$A_F = is8(2\pi)^5 \frac{\sqrt{2\pi}}{[2ay]^{1/2}} \Phi_{0F}^2 e^{y\chi_0}, \quad (20)$$

while in the non-forward case we have

$$A_{NF} = is8(2\pi)^5 \frac{\sqrt{2\pi}}{[2ay]^{3/2}} \Phi_{0NF}^2 e^{y\chi_0}. \quad (21)$$

The transition between the non-forward and the forward region is a delicate matter. The different large- $y$  behavior ( $y^{-1/2}$  and  $y^{-3/2}$ ) of the  $A_F$  and  $A_{NF}$  amplitudes originates from the different small- $\nu$  behavior (note, in particular, the  $1/\nu$  singularity in the forward impact factor (18)). As we will show in the Appendix B, this  $1/\nu$  singularity comes from the large- $r_0$  domain, and it reflects the perturbative nature of the BFKL Pomeron. In particular, it is related to the singularity of the perturbative gluon propagator at zero momentum, and it must disappear after the introduction of an appropriate infrared cutoff<sup>3</sup>. Considering the elastic scattering amplitude as a function of the momentum transfer  $t$ , the difference in the small- $\nu$  behavior of the non-forward and the forward results leads to a cusp at  $t = 0$ : the

---

<sup>3</sup>This was demonstrate using a simplified form of the BFKL kernel in [18, 19].

elastic cross section (2) has a finite limit at  $t = 0$ , but its  $t$ -derivative at  $t = 0$  is infinite. Generally speaking, in the BFKL approximation the point  $t = 0$  exhibits the perturbative nature most explicitly, and changes from perturbative to nonperturbative QCD are expected to be most dramatic in this kinematic region.

After these general remarks we are now able to extract, by comparing (20) and (21) with (1), the Regge residue factors  $g_F$  and  $g_{NF}$ :

$$\begin{aligned} g_F &= 2^{3/2} \Phi_{0F} (2\pi)^{5/2} \left( \frac{2\pi}{2ay} \right)^{\frac{1}{4}} \\ g_{NF} &= 2^{3/2} \Phi_{0NF} (2\pi)^{5/2} \left( \frac{2\pi}{(2ay)^3} \right)^{\frac{1}{4}} \end{aligned} \quad (22)$$

The fact that these couplings have a residual  $y$ -dependence is a consequence of the branch cut nature of the BFKL singularity in the angular momentum plane: eqs.(1) -(3) are valid for Regge poles. We shall use these relations in the next section in order to extract the triple Pomeron vertex  $g_{3P}$ .

### 3 Triple Pomeron amplitude

Having collected all necessary ingredients we now turn to the central topic of this study, the triple Pomeron vertex. We again start from the Regge form for the diffractive cross section in the triple Regge region, assuming Regge pole singularities in all three exchange channels. The cross section is obtained from the 6-point amplitude (Fig.2) by taking the discontinuity in the diffractive mass squared,  $M^2$ . We define

$$M^2 \frac{d\sigma^{(diff)}}{dt dM^2} = \frac{1}{8\pi^2 s} a_6; \quad (23)$$

Regge theory gives

$$\begin{aligned} M^2 \frac{d\sigma^{(diff)}}{dt dM^2} &= \frac{1}{16\pi^2} |e^{-i\frac{\pi}{2}\alpha(t)}|^2 g_N^3 g_{3P} \left( \frac{s}{M^2} \right)^{2\alpha(t)-2} \left( \frac{M^2}{s_0} \right)^{\alpha(0)-1} \\ &= \frac{1}{16\pi^2} |e^{-i\frac{\pi}{2}\alpha(t)}|^2 g_F g_{NF}^2 g_{3P} \left( \frac{s}{M^2} \right)^{2\alpha(t)-2} \left( \frac{M^2}{s_0} \right)^{\alpha(0)-1} \end{aligned} \quad (24)$$

where  $g_{3P}$  is the triple Pomeron vertex,  $t$  denotes the momentum transfer, and  $s_0$  is an energy scale. The triple Pomeron vertex depends upon  $t$ . It will also be convenient to introduce the rapidity variable  $Y = \log(s/s_0)$  and the rapidity interval of the diffractive states  $Y_M = \log(M^2/s_0)$ . It will be our aim to extract the counterpart of  $g_{3P}$  in the framework of perturbative QCD (by analyzing, in the leading log approximation, the analogous high energy limit in perturbative QCD), and to compare its value with the empirical value in  $pp$  scattering. To this end we consider a (hypothetical) process in the triple Regge region, e.g.  $\gamma^* \gamma^* \rightarrow X \gamma^*$ , for which the use of perturbative QCD can be justified. Because of Regge factorization, the value of the triple Pomeron vertex will be independent of the external particles (e.g.  $\gamma^*$  with virtuality  $Q^2$ ).

### 3.1 The QCD amplitude

Let us look at the analysis [6] of QCD Feynman diagrams in the leading log  $s$  approximation and recapitulate the main results. To this end we write the general integral representation for the differential cross section of the  $3 \rightarrow 3$  process in Fig. 2 (see eq. (2.2) in [6])

$$M^2 \frac{d\sigma^{(diff)}}{dt dM^2} = \frac{1}{16\pi} \int \frac{d\omega}{2\pi i} \int \frac{d\omega_1}{2\pi i} \int \frac{d\omega_2}{2\pi i} \left(\frac{M^2}{Q^2}\right)^\omega \left(\frac{s}{M^2}\right)^{\omega_1+\omega_2} \xi_{\omega_1} \xi_{\omega_2}^* F(\omega, \omega_1, \omega_2, 0, t, t), \quad (25)$$

where the  $\xi_{\omega_i}$  are signature factors.

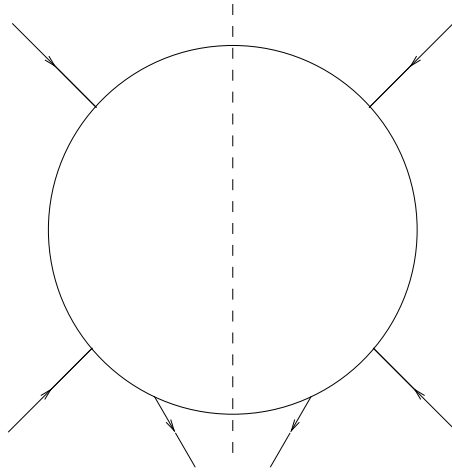


Figure 2: Diffractive amplitude

The differential cross section (25) can be represented by diagrams built from reggeized gluons. The set of diagrams which is of particular interest for us is illustrated in Fig.3a: ellipses denote impact factors, circles the two-gluon BFKL Green's function, and the triangle the  $2 \rightarrow 4$  gluon vertex. The shaded box denotes the evolution of the 4 gluon state, mediated by the sum over all pairwise interactions between the four reggeized gluons. The last interaction (in Fig.3a: the lowest one) has to connect one of the two reggeized gluons on the lhs with one of the gluons on the rhs. Let us briefly recapitulate how this result is obtained. The analysis of Feynman diagrams in the high energy limit leads to gluon amplitudes  $D_2$ ,  $D_3$ , and  $D_4$  which satisfy a set of coupled integral equations (Fig.4). These functions are nonamputated, i.e. they contain reggeon denominators for the outgoing (reggeized) gluon states. Removal (amputation) of these reggeon denominators leads to the corresponding functions  $C_i$  ( $i = 2, 3, 4$ ). For example,

$$D_4^{(\omega)} = \frac{C_4^{(\omega)}}{\omega - \beta_1 - \beta_2 - \beta_3 - \beta_4}. \quad (26)$$

In order to obtain the partial wave  $F$  of the triple Regge cross section, we attach two  $2 \rightarrow 2$  BFKL Green's functions to the amputated function  $C_4$ , one for the two outgoing gluons on



the lhs, another one for the two gluons on the rhs. In order to avoid double counting we have to require that the last interaction inside the four-gluon state has to connect one of the two gluons on the lhs with one of the gluons on the rhs. As a result, we arrive at the following expression for the partial wave  $F$  in the triple Regge cross section formula:

$$F = \left[ C_4^{(\omega)} - \frac{C_4^{(\omega)} \otimes V_{2 \rightarrow 2}(12)}{\omega - \beta_{1'} - \beta_{2'} - \beta_3 - \beta_4} - \frac{C_4^{(\omega)} \otimes V_{2 \rightarrow 2}(34)}{\omega - \beta_1 - \beta_2 - \beta_{3'} - \beta_{4'}} \right] \otimes G_{2 \rightarrow 2}(12, \omega_1) G_{2 \rightarrow 2}(34, \omega_2), \quad (27)$$

where  $\beta_i$  are the trajectories of the reggeized gluons,  $V_{2 \rightarrow 2}$  is the BFKL kernel (without the gluon trajectory function, but including its tensor color structure, here acting for the pairs (12) and (34) which are in a color singlet state), and  $G_{2 \rightarrow 2}$  denotes the full non forward BFKL Green function. A convenient way to rewrite  $F$  in terms of  $D_4$  is:

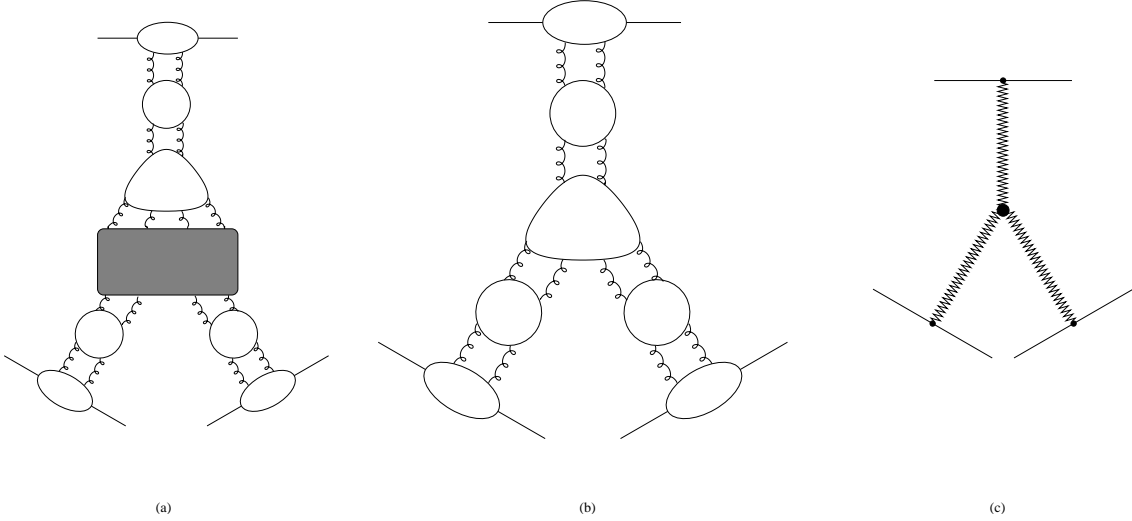


Figure 3: Triple interaction

$$F = \left[ D_4^{(\omega)} \otimes (\omega - H_4) + D_4^{(\omega)} \otimes (V(13) + V(14) + V(23) + V(24)) \right] \otimes G_{2 \rightarrow 2}(12, \omega_1) G_{2 \rightarrow 2}(34, \omega_2), \quad (28)$$

where  $H_4$  is the standard BKP evolution operator for the 4-gluon state.

As the last step, one has to apply a reduction procedure to the amplitude  $D_4$ . As a part of the coupled integral equations,  $D_4$  still contains reggeizing pieces: the outgoing four gluon state may contain configurations where a pair of two gluons is in an antisymmetric color octet configuration, which satisfies the BFKL bootstrap condition and collapses into a single gluon. It is convenient to remove these configurations, i.e. to define amplitudes  $D_4^I$  which are irreducible with respect to the bootstrap property. This reduction has been described in [6], and  $D_4$  decomposes into the two terms  $D_4 = D_4^R + D_4^I$ , separating the reggeizing (R) and irreducible (I) parts. In (28), let us first consider the irreducible part,  $D_4^I$ . As shown in [6],  $D_4^I$  consists of the diagrams of Fig.3a which we have described before. The triangle - with

two gluons entering from above and four gluons leaving below - defines the triple Pomeron vertex, and its structure is quite simple:

$$\delta_{bb'} (\delta_{a_1 a_2} \delta_{a_3 a_4} V(12, 34) + \delta_{a_1 a_3} \delta_{a_2 a_4} V(13, 24) + \delta_{a_1 a_4} \delta_{a_2 a_3} V(14, 23)), \quad (29)$$

where the  $b, b'$  are the color labels of the reggeized gluons of the ladder above the triple Pomeron vertex,  $a_i$  the color indices of the reggeized gluons inside the two lower ladders (counting from left to right), and the arguments of the function  $V$  refer to the momenta of the gluons. Below this vertex, before the two gluons on the lhs and the two gluons on the rhs are restricted to color singlet states and branch into the two disjoint BFKL Green's functions, all pairwise interactions between the four gluons have to be summed. However, it is easy to see that any rung between two color singlet two-gluon states costs a suppression factor of the order  $1/N_c^2$ : in the large- $N_c$  limit, therefore, in Fig.3a the interaction inside the shaded area can be neglected, and we are left with the diagrams of Fig.3b. In (28), the factor  $\omega - H_4$  cancels the evolution inside  $D_4^R$ , and the terms proportional to  $V(13)$  etc. drop out. In (29), only the first term contributes to the large- $N_c$  limit.

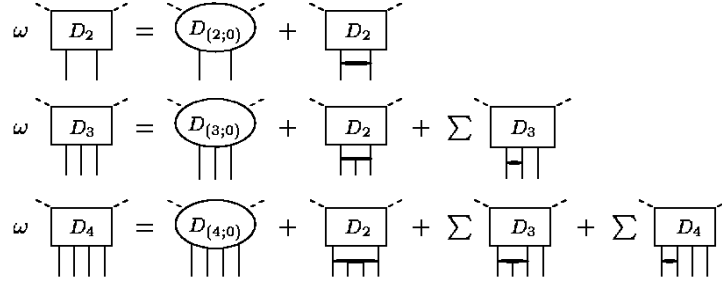


Figure 4: Chained equations for the multi reggeized gluon amplitudes.

Before we write down the explicit expression for these diagrams, a few words about the contribution of  $D_4^R$ . It is convenient to go back to (26) and (27). Since  $D_4^R$  is nothing but a BFKL ladder in which, at the lower end, the reggeized gluons split into two (or three) elementary gluons, it provides an extra contribution to the triple Pomeron vertex. From the color structure of  $D_4^R$ , given in [6], eq.(4.3), it can be shown that this contribution is subleading in  $1/N_c$ . In conclusion, the large- $N_c$  limit therefore reduces the diffractive cross section, given in [6], to the diagrams shown in Fig.3b which is very similar to the ‘Regge pole’ diagrams of Fig.3c.

### 3.2 Extraction of the triple Pomeron vertex

Let us write down the analytic expression for the the generalized six point amplitude  $a_6$ :

$$a_6 = 2s \int \frac{d^2 \mathbf{q}}{(2\pi)^3} \frac{d^2 \mathbf{q}_1' d^2 \mathbf{q}_2'}{(2\pi)^3} \delta^{(2)}(\mathbf{l}_\alpha - \mathbf{q}_1' - \mathbf{q}_2') \Phi_\alpha(\mathbf{q}, \mathbf{l}_\alpha - \mathbf{q}) \tilde{G}_2^{(A)}(Y_M | \mathbf{q}, \mathbf{l}_\alpha - \mathbf{q}; \mathbf{q}_1', \mathbf{q}_2')$$

$$\int \frac{d^2 \mathbf{k}_1 d^2 \mathbf{k}_2}{(2\pi)^3} \delta^{(2)}(\mathbf{l}_\beta - \mathbf{k}_1 - \mathbf{k}_2) \frac{d^2 \mathbf{k}_3 d^2 \mathbf{k}_4}{(2\pi)^3} \delta^{(2)}(\mathbf{l}_\gamma - \mathbf{k}_3 - \mathbf{k}_4) V_{2 \rightarrow 4}(\mathbf{q}_1', \mathbf{q}_2' | \mathbf{k}_1, \mathbf{k}_2; \mathbf{k}_3, \mathbf{k}_4)$$

$$\begin{aligned}
& \int \frac{d^2 \mathbf{k}'_1}{(2\pi)^3} \tilde{G}_2^{(NA)}(Y - Y_M | \mathbf{k}_1, \mathbf{k}_2; \mathbf{k}_{1'}, \mathbf{l}_\beta - \mathbf{k}_{1'}) \Phi_\beta(\mathbf{k}_{1'}, \mathbf{l}_\beta - \mathbf{k}_{1'}) \\
& \int \frac{d^2 \mathbf{k}'_3}{(2\pi)^3} \tilde{G}_2^{(NA)}(Y - Y_M | \mathbf{k}_3, \mathbf{k}_4; \mathbf{k}_{3'}, \mathbf{l}_\gamma - \mathbf{k}_{3'}) \Phi_\gamma(\mathbf{k}_{3'}, \mathbf{l}_\gamma - \mathbf{k}_{3'}), \tag{30}
\end{aligned}$$

where  $\mathbf{l}_i$  (with  $\mathbf{l}_i^2 - t_i$ ) are the momentum transfers through the impacts factor  $\Phi_i$ . Later, on we will take  $t_\alpha = 0$  and define the triple Regge cross section.

Following the procedure of the previous section, we perform the Fourier transform for the  $t_\alpha$ -channel (last two lines in (30)); we write a representation of  $\delta^{(2)}(\mathbf{l}_\alpha - \mathbf{q}_{1'} - \mathbf{q}_{2'})$  together with the Green function in the last line, see(15), to obtain

$$\begin{aligned}
\delta^{(2)}(\mathbf{l}_\alpha - \mathbf{q}_{1'} - \mathbf{q}_{2'}) \tilde{G}_2^{(A)}(Y_M | \mathbf{q}, \mathbf{l}_\alpha - \mathbf{q}; \mathbf{q}_{1'}, \mathbf{q}_{2'}) &= (2\pi)^3 \int d\mu_0 e^{Y_M \chi(h_0)} N_{h_0} \times \\
& \int d^2 \boldsymbol{\rho}_\alpha e^{-i \boldsymbol{\rho}_\alpha \cdot (\mathbf{l}_\alpha - \mathbf{q}_{1'} - \mathbf{q}_{2'})} |\mathbf{q}_{1'}|^2 |\mathbf{q}_{2'}|^2 \tilde{E}_{h_\alpha, \bar{h}_\alpha}(\mathbf{q}, \mathbf{l}_\alpha - \mathbf{q}) \tilde{E}_{h_\alpha, \bar{h}_\alpha}^*(\mathbf{q}_{1'}, \mathbf{q}_{2'}). \tag{31}
\end{aligned}$$

The other two  $t$ -channels with their (non amputated) Green functions and  $\delta$  distribution can be rewritten in a similar way (using an expansion in the conformal weights  $h_\beta$  and  $h_\gamma$ ); the only difference is the absence of the factors  $|\mathbf{k}_{1'}|^2 |\mathbf{l}_\beta - \mathbf{k}_{1'}|^2$  and  $|\mathbf{k}_{3'}|^2 |\mathbf{l}_\gamma - \mathbf{k}_{3'}|^2$ . Using the conformal representation of the impact factors  $\Phi_i^{h_i}(\mathbf{l}_i)$  for  $i = \alpha, \beta, \gamma$  given in (17), we obtain the following expression for (30):

$$\begin{aligned}
a_6 &= 2s \int d\mu_\alpha d\mu_\beta d\mu_\gamma e^{Y_M \chi(h_\alpha) + (Y - Y_M)(\chi(h_\beta) + \chi(h_\gamma))} N_{h_\alpha} N_{h_\beta} N_{h_\gamma} \Phi_\alpha^{h_\alpha} \Phi_\beta^{h_\beta} \Phi_\gamma^{h_\gamma} \int \prod_{i=\alpha, \beta, \gamma} d^2 \boldsymbol{\rho}_i \times \\
& e^{i(\boldsymbol{\rho}_\beta \cdot \mathbf{l}_\beta + \boldsymbol{\rho}_\gamma \cdot \mathbf{l}_\gamma - \boldsymbol{\rho}_\alpha \cdot \mathbf{l}_\alpha)} \int \prod_{j=1}^4 d^2 \mathbf{k}_j \tilde{E}_{h_\beta, \bar{h}_\beta}(\mathbf{k}_1, \mathbf{k}_2) e^{-i \boldsymbol{\rho}_\beta \cdot (\mathbf{k}_1 + \mathbf{k}_2)} \tilde{E}_{h_\gamma, \bar{h}_\gamma}(\mathbf{k}_3, \mathbf{k}_4) e^{-i \boldsymbol{\rho}_\gamma \cdot (\mathbf{k}_3 + \mathbf{k}_4)} \times \\
& \left( \int d^2 \mathbf{q}_{1'} d^2 \mathbf{q}_{2'} V_{2 \rightarrow 4}(\mathbf{q}_{1'}, \mathbf{q}_{2'} | \mathbf{k}_1, \mathbf{k}_2; \mathbf{k}_3, \mathbf{k}_4) |\mathbf{q}_{1'}|^2 |\mathbf{q}_{2'}|^2 \tilde{E}_{h_\alpha, \bar{h}_\alpha}^*(\mathbf{q}_{1'}, \mathbf{q}_{2'}) e^{i \boldsymbol{\rho}_\alpha \cdot (\mathbf{q}_{1'} + \mathbf{q}_{2'})} \right) \tag{32}
\end{aligned}$$

Before we evaluate the Fourier transform of the last line in (32), we note several simplifications. First, the  $2 \rightarrow 4$  vertex will be simplified by the fact that the gluons (1, 2) and (3, 4) couple to two BFKL pomerons in color singlet states. This fact considerably reduces the number of contributions coming from  $V_{2 \rightarrow 4}$ : only four identical contributions are left. Next, we restrict ourselves to the large  $N_c$  limit which eliminates the nonplanar part of the  $2 \rightarrow 4$  vertex. As a result of these simplifications we can write:

$$\begin{aligned}
& \int d^2 \mathbf{q}_{1'} d^2 \mathbf{q}_{2'} V_{2 \rightarrow 4}(\mathbf{q}_{1'}, \mathbf{q}_{2'} | \mathbf{k}_1, \mathbf{k}_2; \mathbf{k}_3, \mathbf{k}_4) |\mathbf{q}_{1'}|^2 |\mathbf{q}_{2'}|^2 E_{h, \bar{h}}^*(\mathbf{q}_{1'}, \mathbf{q}_{2'}) = \\
& C_{1V} \int d^2 \mathbf{q}_{1'} d^2 \mathbf{q}_{2'} A_{2 \rightarrow 3}(\mathbf{k}_1, \mathbf{k}_2 + \mathbf{k}_3, \mathbf{k}_4 | \mathbf{q}_{1'}, \mathbf{q}_{2'}) |\mathbf{q}_{1'}|^2 |\mathbf{q}_{2'}|^2 \tilde{E}_{h, \bar{h}}^*(\mathbf{q}_{1'}, \mathbf{q}_{2'}) \tag{33}
\end{aligned}$$

where the constant

$$C_{1V} = 4 \frac{\pi^{3/2}}{32} g^4 \frac{(2N_c)^2}{\sqrt{N_c^2 - 1}} = \frac{\pi^{3/2}}{2} g^4 \frac{N_c^2}{\sqrt{N_c^2 - 1}} \approx 2^3 \pi^{7/2} \alpha_s^2 N_c, \tag{34}$$

follows from our choice of the normalizations we have made for the integration measure and for the impact factors. Details are given in appendix A. As to the color factors, we keep only the leading term in the large  $N_c$  limit.

After performing the Fourier transform of the last line in (32) [7, 8] (i.e. performing the transition  $\mathbf{k}_i \rightarrow \boldsymbol{\rho}_i$ ) one obtains for the triple Pomeron coupling <sup>4</sup>

$$\begin{aligned} & \frac{C_{1V}}{(2\pi)^4} \delta^{(2)}(\boldsymbol{\rho}_{23}) \frac{|\rho_{14}|^2}{|\rho_{12}|^2 |\rho_{24}|^2} |\boldsymbol{\rho}_1|^2 |\boldsymbol{\rho}_2|^2 E_{h_\alpha, \bar{h}_\alpha}^*(\rho_{1\alpha}, \rho_{4\alpha}) = \\ & \frac{C_{1V}}{(2\pi)^4} \delta^{(2)}(\boldsymbol{\rho}_{23}) 16 h_\alpha \bar{h}_\alpha (1 - h_\alpha) (1 - \bar{h}_\alpha) \frac{1}{|\rho_{12}|^2 |\rho_{24}|^2 |\rho_{41}|^2} E_{h_\alpha, \bar{h}_\alpha}^*(\rho_{1\alpha}, \rho_{4\alpha}) \end{aligned} \quad (35)$$

The Fourier transform of the remaining  $\mathbf{k}_i$  dependent part is easily done and leads to the two factors  $E_{h_\beta, \bar{h}_\beta}(\rho_{1\beta}, \rho_{2\beta})$  and  $E_{h_\gamma, \bar{h}_\gamma}(\rho_{3\gamma}, \rho_{4\gamma})$ .

As a result, we can write

$$\begin{aligned} a_6 = & 2s C_{2V} \int d\mu_\alpha d\mu_\beta d\mu_\gamma e^{Y_M \chi(h_\alpha) + (Y - Y_M)(\chi(h_\beta) + \chi(h_\gamma))} N_{h_\alpha} N_{h_\beta} N_{h_\gamma} \Phi_\alpha^{h_\alpha} \Phi_\beta^{h_\beta} \Phi_\gamma^{h_\gamma} \times \\ & 16 h_\alpha \bar{h}_\alpha (1 - h_\alpha) (1 - \bar{h}_\alpha) \int \prod_{i=\alpha, \beta, \gamma} d^2 \boldsymbol{\rho}_i e^{i(\boldsymbol{\rho}_\beta \cdot \mathbf{l}_\beta + \boldsymbol{\rho}_\gamma \cdot \mathbf{l}_\gamma - \boldsymbol{\rho}_\alpha \cdot \mathbf{l}_\alpha)} \times \\ & \int \frac{d^2 \boldsymbol{\rho}_1 d^2 \boldsymbol{\rho}_2 d^2 \boldsymbol{\rho}_4}{|\rho_{12}|^2 |\rho_{24}|^2 |\rho_{41}|^2} E_{h_\beta, \bar{h}_\beta}(\rho_{1\beta}, \rho_{2\beta}) E_{h_\gamma, \bar{h}_\gamma}(\rho_{2\gamma}, \rho_{4\gamma}) E_{h_\alpha, \bar{h}_\alpha}^*(\rho_{4\alpha}, \rho_{1\alpha}), \end{aligned} \quad (36)$$

where  $C_{2V} = C_{1V}/(2\pi)^4$ .

The integral in the last line of (36) has been calculated explicitly in [13, 12], where the conformal invariance has been used explicitly. The result can be written in the form

$$\Omega(1 - h_\alpha, h_\beta, h_\gamma) \left( \rho_{\alpha\beta}^{-\Delta_{\alpha\beta 01}} \rho_{\alpha\gamma}^{-\Delta_{\alpha\gamma}} \rho_{\beta\gamma}^{-\Delta_{\beta\gamma}} \times (h.c.) \right) \quad (37)$$

where the function  $\Omega$  can be found in [13, 12]. The exponents are defined for the general conformal covariant three point function:  $\Delta_{ij} = h_i + h_j - h_{k \neq i, j}$  and remembering to use for the index 0 the weight  $(1 - h_\alpha) = \bar{h}_\alpha^*$ , which is due to the fact that one function is complex conjugated. That means  $\Delta_{\alpha\beta} = 1 - h_\alpha + h_\beta - h_\gamma$ , etc.

We shall now consider the limit  $\mathbf{l}_\alpha = 0$  (keeping  $t_\beta = -\mathbf{l}_\beta^2$  and  $t_\gamma = -\mathbf{l}_\gamma^2$  still independent from each other) and perform the remaining  $\boldsymbol{\rho}$  integrals still present in (36). Explicitly we have to calculate:

$$I_c = \int d^2 \boldsymbol{\rho}_\alpha d^2 \boldsymbol{\rho}_\beta d^2 \boldsymbol{\rho}_\gamma \left( \rho_{\alpha\beta}^{-\Delta_{\alpha\beta}} \rho_{\alpha\gamma}^{-\Delta_{\alpha\gamma}} \rho_{\beta\gamma}^{-\Delta_{\beta\gamma}} \times (h.c.) \right) e^{i\boldsymbol{\rho}_\beta \cdot \mathbf{l}_\beta + i\boldsymbol{\rho}_\gamma \cdot \mathbf{l}_\gamma} \quad (38)$$

The integration over  $\boldsymbol{\rho}_\alpha$  can be done easily:

$$\int d^2 \boldsymbol{\rho}_\alpha \left( \rho_{\alpha\beta}^{-\Delta_{\alpha\beta}} \rho_{\alpha\gamma}^{-\Delta_{\alpha\gamma}} \times (h.c.) \right) = f(h_\alpha, h_\beta, h_\gamma) \left( \rho_{\gamma\beta}^{1 - \Delta_{\alpha\beta} - \Delta_{\alpha\gamma}} \times (h.c.) \right) \quad (39)$$

---

<sup>4</sup>Comparing with an analogous expression in [12], we differ in the Casimir operators which are not present in [12]

where

$$\begin{aligned}
f(h_\alpha, h_\beta, h_\gamma) &= -(-1)^{\Delta_{\alpha\gamma} - \Delta_{\alpha\beta}} \frac{\Gamma(1 - \Delta_{\alpha\beta})\Gamma(1 - \Delta_{\alpha\gamma})}{\Gamma(2 - \Delta_{\alpha\beta} - \Delta_{\alpha\gamma})} \frac{\Gamma(1 - \bar{\Delta}_{\alpha\beta})\Gamma(1 - \bar{\Delta}_{\alpha\gamma})}{\Gamma(2 - \bar{\Delta}_{\alpha\beta} - \bar{\Delta}_{\alpha\gamma})} \frac{\sin(\pi\Delta_{\alpha\beta}) \sin(\pi\Delta_{\alpha\gamma})}{\sin(\pi(\Delta_{\alpha\beta} + \Delta_{\alpha\gamma}))} \\
&= -(-1)^{2(h_\gamma - h_\beta)} \frac{\Gamma(h_\alpha - h_\beta + h_\gamma)\Gamma(h_\alpha - h_\gamma + h_\beta)}{\Gamma(2h_\alpha)} \frac{\Gamma(\bar{h}_\alpha - \bar{h}_\beta + \bar{h}_\gamma)\Gamma(\bar{h}_\alpha - \bar{h}_\gamma + \bar{h}_\beta)}{\Gamma(2\bar{h}_\alpha)} \times \\
&\quad \frac{\sin(\pi(h_\alpha - h_\beta + h_\gamma)) \sin(\pi(h_\alpha - h_\gamma + h_\beta))}{\sin(2\pi h_\alpha)} \tag{40}
\end{aligned}$$

Therefore one is left with the following integration

$$I_c = (-1)^{\Delta_{\beta\gamma} + \bar{\Delta}_{\beta\gamma}} f(h_\alpha, h_\beta, h_\gamma) \int d^2\rho_\beta d^2\rho_\gamma \left( \rho_\gamma^{1 - \Delta_{\alpha\beta} - \Delta_{\alpha\gamma} - \Delta_{\beta\gamma}} \times (h.c.) \right) e^{i\rho_\beta \mathbf{l}_\beta + i\rho_\gamma \mathbf{l}_\gamma}. \tag{41}$$

Performing a shift in one of the integration variables, one integration can be done to extract the momentum conserving  $\delta$  function:

$$I_c = (2\pi)^2 \delta^{(2)}(\mathbf{l}_\beta + \mathbf{l}_\gamma) (-1)^{\Delta_{\beta\gamma} + \bar{\Delta}_{\beta\gamma}} f(h_\alpha, h_\beta, h_\gamma) \int d^2\rho \left( \rho^{1 - \Delta_{\alpha\beta} - \Delta_{\alpha\gamma} - \Delta_{\beta\gamma}} \times (h.c.) \right) e^{i\rho \mathbf{l}_\beta}. \tag{42}$$

Also the remaining integral can be done easily. Introducing  $\xi = 1 - \Delta_{\alpha\beta} - \Delta_{\alpha\gamma} - \Delta_{\beta\gamma}$  and  $\bar{\xi} = 1 - \bar{\Delta}_{\alpha\beta} - \bar{\Delta}_{\alpha\gamma} - \bar{\Delta}_{\beta\gamma}$ , we have

$$\int d^2\rho \rho^\xi \rho^{*\bar{\xi}} e^{i\rho \mathbf{l}_\beta} = 2\pi i^{\bar{\xi} - \xi} 2^{1 + \xi + \bar{\xi}} \frac{\Gamma(1 + \bar{\xi})}{\Gamma(-\xi)} \mathbf{l}_\beta^{-\bar{\xi} - 1} \mathbf{l}_\beta^{* - \xi - 1} \tag{43}$$

Returning to (38) we have

$$I_c = (2\pi)^3 \delta^{(2)}(\mathbf{l}_\beta + \mathbf{l}_\gamma) f(h_\alpha, h_\beta, h_\gamma) (-1)^{\Delta_{\beta\gamma} + \bar{\Delta}_{\beta\gamma}} i^{\bar{\xi} - \xi} 2^{1 + \xi + \bar{\xi}} \frac{\Gamma(1 + \bar{\xi})}{\Gamma(-\xi)} \mathbf{l}_\beta^{-\bar{\xi} - 1} \mathbf{l}_\beta^{* - \xi - 1} \tag{44}$$

with

$$\xi = 1 - ((1 - h_\alpha) + h_\beta - h_\gamma) - ((1 - h_\alpha) + h_\gamma - h_\beta) - (h_\beta + h_\gamma - (1 - h_\alpha)) = h_\alpha - h_\beta - h_\gamma \tag{45}$$

and

$$\bar{\xi} = \bar{h}_\alpha - \bar{h}_\beta - \bar{h}_\gamma \quad \xi^* = -1 - \bar{h}_\alpha + \bar{h}_\beta + \bar{h}_\gamma \quad \bar{\xi}^* = -1 - h_\alpha + h_\beta + h_\gamma \tag{46}$$

Collecting all this in the formula for the amplitude  $a_6$  in (36), we obtain the result:

$$\begin{aligned}
a_6 &= 2s C_{3V} \int d\mu_\alpha d\mu_\beta d\mu_\gamma e^{Y_M \chi(h_\alpha) + (Y - Y_M)(\chi(h_\beta) + \chi(h_\gamma))} N_{h_\alpha} N_{h_\beta} N_{h_\gamma} \Phi_\alpha^{h_\alpha} \Phi_\beta^{h_\beta^*} \Phi_\gamma^{h_\gamma^*} \times \\
&16h_\alpha \bar{h}_\alpha (1 - h_\alpha) (1 - \bar{h}_\alpha) \Omega(1 - h_\alpha, h_\beta, h_\gamma) f(h_\alpha, h_\beta, h_\gamma) \times \\
&(-1)^{\Delta_{\beta\gamma} + \bar{\Delta}_{\beta\gamma}} i^{\bar{\xi} - \xi} 2^{1 + \xi + \bar{\xi}} \frac{\Gamma(1 + \bar{\xi})}{\Gamma(-\xi)} \mathbf{l}_\beta^{-\bar{\xi} - 1} \mathbf{l}_\beta^{* - \xi - 1} \tag{47}
\end{aligned}$$

Here we have removed the  $\delta^{(2)}(\mathbf{l}_\beta + \mathbf{l}_\gamma)$  function. The constant  $C_{3V}$  has the form

$$C_{3V} = (2\pi)^3 C_{2V} = \frac{C_{1V}}{2\pi} \tag{48}$$

Let us now consider the saddle point approximation, assuming that both  $Y_M$  and  $Y - Y_M$  are large. Following the standard BFKL arguments, the leading contributions will come from the conformal weights being close the value  $1/2$ , i.e. from conformal spin equal to zero and small  $\nu$ 's. In this region we have

$$h_i = \frac{1}{2} + i\nu_i, \quad \xi = -\frac{1}{2} + i(\nu_\alpha - \nu_\beta - \nu_\gamma), \quad (49)$$

and therefore

$$f(h_\alpha, h_\beta, h_\gamma) \approx -1 \times \frac{\Gamma(\frac{1}{2})\Gamma(\frac{1}{2})}{\Gamma(1)} \times \frac{\Gamma(\frac{1}{2})\Gamma(\frac{1}{2})}{\Gamma(1)} \times \frac{1 \times 1}{-\sin 2\pi i\nu_\alpha} \approx -\frac{i\pi}{2\nu_\alpha}, \quad (50)$$

$$\begin{aligned} (-1)^{\Delta_{\beta\gamma} + \bar{\Delta}_{\beta\gamma}} i^{\bar{\xi} - \xi} 2^{\xi + \bar{\xi}} \frac{\Gamma(1 + \bar{\xi})}{\Gamma(-\xi)} \mathbf{l}_\beta^{-\bar{\xi} - 1} \mathbf{l}_\beta^{* - \xi - 1} &\approx -1 \times \frac{1}{2} \frac{\Gamma(\frac{1}{2})}{\Gamma(\frac{1}{2})} \mathbf{l}_\beta^{-\frac{1}{2} - i(\nu_\alpha - \nu_\beta - \nu_\gamma)} \mathbf{l}_\beta^{* - \frac{1}{2} - i(\nu_\alpha - \nu_\beta - \nu_\gamma)} \\ &\approx -\frac{1}{2} |\mathbf{l}_\beta|^{-1 - 2i(\nu_\alpha - \nu_\beta - \nu_\gamma)} \end{aligned} \quad (51)$$

Moreover,  $16h_\alpha(1 - h_\alpha)\bar{h}_\alpha(1 - \bar{h}_\alpha) \approx 1$  and  $N_h \approx 16\nu^2$ . We note that the function  $f$ , near  $\mathbf{l}_\alpha = \mathbf{0}$ , behaves in  $\nu_\alpha$  in the same way as the forward impact factors (18). Therefore, with respect to the  $t_\alpha$  channel we are facing the same problem as discussed in the previous section. Substituting this behaviour in (47) one has

$$\begin{aligned} a_6 &\approx 2s C_{3V} \int d\nu_\alpha d\nu_\beta d\nu_\gamma e^{Y_M \chi(h_\alpha) + (Y - Y_M)(\chi(h_\beta) + \chi(h_\gamma))} 16^3 \nu_\alpha^2 \nu_\beta^2 \nu_\gamma^2 \Phi_\alpha^{h_\alpha} \Phi_\beta^{h_\beta^*} \Phi_\gamma^{h_\gamma^*} \times \\ &\quad \Omega\left(\frac{1}{2}, \frac{1}{2}, \frac{1}{2}\right) \frac{i\pi}{4\nu_\alpha} |\mathbf{l}_\beta|^{-1 - 2i(\nu_\alpha - \nu_\beta - \nu_\gamma)} \\ &= 2is C_{4V} \int d\nu_\alpha d\nu_\beta d\nu_\gamma \nu_\alpha \nu_\beta^2 \nu_\gamma^2 e^{Y_M \chi(h_\alpha) + (Y - Y_M)(\chi(h_\beta) + \chi(h_\gamma))} \Phi_\alpha^{h_\alpha} \times \\ &\quad \Phi_\beta^{h_\beta^*} \Phi_\gamma^{h_\gamma^*} |\mathbf{l}_\beta|^{-1 - 2i(\nu_\alpha - \nu_\beta - \nu_\gamma)} \end{aligned} \quad (52)$$

where

$$C_{4V} = 2^{10} \pi \Omega\left(\frac{1}{2}, \frac{1}{2}, \frac{1}{2}\right) C_{3V} = 2^9 \Omega\left(\frac{1}{2}, \frac{1}{2}, \frac{1}{2}\right) C_{1V} = 2^{12} \pi^{7/2} \alpha_s^2 N_c \Omega\left(\frac{1}{2}, \frac{1}{2}, \frac{1}{2}\right). \quad (53)$$

The numerical value for  $\Omega(\frac{1}{2}, \frac{1}{2}, \frac{1}{2})$  has been found in [13, 12]:

$$\Omega\left(\frac{1}{2}, \frac{1}{2}, \frac{1}{2}\right) = 2\pi^7 {}_4F_3\left(\frac{1}{2}\right) {}_6F_5\left(\frac{1}{2}\right) \approx 7766.679 \quad (54)$$

The remaining part of our saddle point analysis of  $a_6$  is analogous to what has been done in subsection 2.1: the integration over  $\nu_\alpha$  goes with an impact factor in the forward direction, whereas for the two integrations in  $\nu_\beta$  and  $\nu_\gamma$  we have the freedom to vary  $t_\beta$  and  $t_\gamma$ : following our discussion after (21) we chose to stay away from the 'most dangerous' points  $t_\beta = t_\gamma = 0$ , i.e. we perform our comparison in the 'safer' region  $t_\beta = t_\gamma \neq 0$ . Putting  $\mathbf{l}_\beta = \mathbf{l}_\alpha = \mathbf{l}$  and using (18) we find that the dependence in  $\mathbf{l}$  in the dominant contribution,

as selected by the saddle points at  $\nu_\alpha = \nu_\beta = \nu_\gamma = 0$ , is just  $1/|\mathbf{l}|$ . The integrals are trivially done and lead to the result:

$$a_6 \approx 2s \frac{C_{4V}}{|\mathbf{l}|} \left( \frac{\sqrt{2\pi}}{[2aY_M]^{1/2}} \Phi_{0F} e^{Y_M \chi_0} \right) \left( \frac{\sqrt{2\pi}}{[2a(Y - Y_M)]^{3/2}} \Phi_{0NF} e^{(Y - Y_M) \chi_0} \right)^2. \quad (55)$$

Using the relations in (22) for rewriting the impact factors in terms of  $g_F$  and  $g_{NF}$ , we arrive at:

$$a_6 \approx s g_F g_{NF}^2 \frac{C_{4V}}{|\mathbf{l}|} \frac{1}{2^{7/2} (2\pi)^{15/2}} \left( \frac{2\pi}{2aY_M} \right)^{\frac{1}{4}} \left( \frac{2\pi}{[2a(Y - Y_M)]^3} \right)^{\frac{1}{2}} e^{Y_M \chi_0} e^{2(Y - Y_M) \chi_0}. \quad (56)$$

Finally we have to relate the generalized amplitude  $a_6$  to the triple Regge cross section formula:

$$M^2 \frac{d\sigma^{(diff)}}{dt dM^2} = \frac{1}{8\pi^2 s} a_6; \quad (57)$$

Comparing our result with (24), we are able to extract the

$$\begin{aligned} g_{3P} &\approx \frac{C_{4V}}{|\mathbf{l}|} \frac{1}{2^{5/2} (2\pi)^{15/2}} \left( \frac{2\pi}{2aY_M} \right)^{\frac{1}{4}} \left( \frac{2\pi}{[2a(Y - Y_M)]^3} \right)^{\frac{1}{2}} \\ &= \frac{1}{|\mathbf{l}|} \frac{2^6}{(2\pi)^4} \alpha_s^2 N_c \Omega \left( \frac{1}{2}, \frac{1}{2}, \frac{1}{2} \right) \left( \frac{2\pi}{2aY_M} \right)^{\frac{1}{4}} \left( \frac{2\pi}{[2a(Y - Y_M)]^3} \right)^{\frac{1}{2}}. \end{aligned} \quad (58)$$

We note that this expression is proportional to  $\alpha_s^{1/4}$ , i.e. there is a very mild dependence on the strong coupling. Considering  $\alpha_s \approx 0.3$  we get

$$g_{3P} \approx \frac{6.5}{Y_M^{1/4} (Y - Y_M)^{3/2}} \frac{1}{|\mathbf{l}|}. \quad (59)$$

The strong dependence upon the momentum transfer near  $\mathbf{l} = 0$  which is closely connected with the perturbative zero mass gluon confirms our expectation that a comparison between perturbative and nonperturbative Regge parameters can be done only in the region of finite momentum transfer, and one cannot expect more than an order-of-magnitude estimate.

Let us comment on other results of this vertex contained in the literature. Within the dipole picture the triple Pomeron has been derived in [10]: an expression for the triple Pomeron coupling can be derived from eq.(61), but no explicit expression or numerical number  $V_0$  has been given in this paper. In [12] explicit expressions for the triple Pomeron vertex can be found: our result disagrees, both in the energy dependence and in the overall normalization. The result of [14] is closest to ours, but, again, we disagree in the overall normalization and in the energy dependence.

## 4 The Pomeron self energy

As an important application of the triple Pomeron coupling we estimate the size of the Pomeron self energy inside a  $2 \rightarrow 2$  scattering amplitude. To this end we replace, in the

amplitude  $a_6$  of the previous section, the two impact factors  $\Phi_\beta^{h_\beta}$  and  $\Phi_\gamma^{h_\gamma}$  by another triple Pomeron vertex  $V_{2 \rightarrow 4}$  which through a BFKL Pomeron and another impact factor couples to the lower external particle. As a modification of  $a_6$ , one has to consider an additional momentum integration over the Pomeron loop, in the momentum variable  $\mathbf{l}_\beta = \mathbf{l}_\alpha - \mathbf{l}_\gamma$ . For simplicity we will restrict ourselves to the forward direction  $\mathbf{l}_\alpha = 0$ . Denoting by  $\xi'$  the same combination (39) of conformal weights as  $\xi$ , with  $h_\alpha$  being replaced by  $h_{\alpha'}$ , the  $\mathbf{l}_\beta$  integral can be carried out and leads to the conservation of the conformal weights above and below the Pomeron loop:

$$\begin{aligned}
& \int d^2 \mathbf{l}_\beta \left( \mathbf{l}_\beta^{-\bar{\xi}-1} \mathbf{l}_\beta^{*-\xi-1} \right) \left( \mathbf{l}_\beta^{-\bar{\xi}'-1} \mathbf{l}_\beta^{*-\xi'-1} \right)^* = \\
& \int d^2 \mathbf{l}_\beta \left( \mathbf{l}_\beta^{-\bar{h}_\alpha + \bar{h}_\beta + \bar{h}_\gamma - 1} \mathbf{l}_\beta^{* - h_\alpha + h_\beta + h_\gamma - 1} \right) \left( \mathbf{l}_\beta^{* h_{\alpha'} - h_\beta - h_\gamma} \mathbf{l}_\beta^{\bar{h}_{\alpha'} - \bar{h}_\beta - \bar{h}_\gamma} \right) = \\
& \int d^2 \mathbf{l}_\beta \mathbf{l}_\beta^{\bar{h}_{\alpha'} - \bar{h}_\alpha - 1} \mathbf{l}_\beta^{* h_{\alpha'} - h_\alpha - 1} = \frac{(2\pi)^2}{2} \delta_{n_\alpha n_{\alpha'}} \delta(\nu_\alpha - \nu_{\alpha'}) .
\end{aligned} \tag{60}$$

Another important ingredient to the Pomeron self energy is the minus sign relative to the BFKL amplitude (5).

We want to evaluate this loop correction to the elastic scattering amplitude, using again the saddle point approximation. Starting from the expression (52), inserting the result (60) and performing the  $\nu_{\alpha'}$  integration, we can write

$$\begin{aligned}
\Delta A_{el}^{LL} &= -i \frac{(2\pi)^2}{2} \frac{s}{4(2\pi)^4} \left( \frac{C_{4V}}{16(2\pi)^5} \right)^2 \int dY_1 dY_2 \times \\
& \int d\nu_\alpha \Phi_\alpha^{h_\alpha} \nu_\alpha^2 \Phi_\alpha^{h_{\alpha'}} e^{(Y_1+Y_2)\chi(\nu_\alpha)} \left( \int d\nu \nu^2 e^{(Y-Y_1-Y_2)\chi(\nu)} \right)^2 ,
\end{aligned} \tag{61}$$

noting that the  $\nu_\beta$  and  $\nu_\gamma$  integrations give identical factors. Let us also note that all the rapidity intervals must be large enough to allow the application of the leading log approximation. This expression can be compared with a similar result in [12]. The remaining  $\nu$  integrations give:

$$\begin{aligned}
\Delta A_{el}^{LL} &= -i \frac{s}{2} \left( \frac{C_{4V}}{2^5(2\pi)^6} \right)^2 \Phi_{0F}^2 \int dY_1 dY_2 e^{\chi_0(Y_1+Y_2)} \left( \frac{2\pi}{2a(Y_1+Y_2)} \right)^{\frac{1}{2}} \\
& e^{2\chi_0(Y-Y_1-Y_2)} \frac{2\pi}{[2a(Y-Y_1-Y_2)]^3}
\end{aligned} \tag{62}$$

This result represents the one loop self energy correction to the BFKL approximation (20). Apart from the fractional powers of  $\alpha_s$  in front of the rapidity factors, the overall power of  $\alpha_s$  inside the  $C_{4V}$ -factors is  $\alpha_s^4$ : compared to the LL BFKL approximation our expression is down by two powers of  $\alpha_s$ , i.e. the self energy correction belongs to NNLO and thus is beyond the NLO corrections calculated recently. Note, however, the exponent  $2\chi_0$  in the last line: for large rapidity intervals  $Y - Y_1 - Y_2$  this energy factor renders the one-loop self energy correction more important than the NLO corrections to the BFKL kernel.



## 5 Numerical estimates

### 5.1 Triple Pomeron vertex

In this final part of our study we use our analytical formulae to obtain numerical estimates. We begin with the phenomenological vertex extracted from the  $pp \rightarrow p + X$  data in the framework of the old triple-Regge analysis [21, 22] and compare with the perturbative triple-Pomeron vertex  $g_{3P}$ .

It was observed that the  $t$ -dependence of the triple-Pomeron contribution to the diffractive dissociation cross section is consistent with the  $t$ -behaviour of the proton-Pomeron vertex square; that is  $M^2 d\sigma/dtdM^2 \propto g_N^2(t)$ . Hence the  $t = -l^2$ -dependence of the triple-Pomeron vertex  $g_{3P}(t)$  must be small; for the  $t$ -slope of  $g_{3P}$  we estimate  $B_{3P} < 1 \text{ GeV}^2$ . Therefore we may consider relatively large  $|l| \sim 1 - 2 \text{ GeV}$  where, in the perturbative calculation, we are away from the QCD dangerous region  $\mathbf{l} = \mathbf{0}$ . In our normalization the phenomenological analysis gives [21, 22]

$$g_{3P} \sim 0.5 - 1 \text{ GeV}^{-1}. \quad (63)$$

Note that when applying our formula (23) to experimental data and extracting a numerical value for the triple-Pomeron vertex, this vertex has to be viewed as an *effective* vertex, i.e. it already accounts for screening corrections due to multi-Pomeron cuts. So the bare vertex may be larger by a factor of about up to  $2 - 4$ <sup>5</sup>. Thus, at the experiment we "observe" a bare vertex of the order  $g_{3P} \sim 2 \text{ GeV}^{-1}$ . This value corresponds to the events with a gap size  $\Delta Y = \ln(s/M^2) = Y - Y_M$  between 3 and 5.

Turning to the perturbative analysis, we first note that, in order to justify the saddle point evaluation of our integrals, we need  $\Delta Y > 4$ . This is just the region of  $z = y\alpha_s N_c/\pi > 1$  where the asymptotic component of the BFKL solution (with conformal spin  $n = 0$ ) starts to exceed the lowest order two-gluon exchange contribution. At the same time the width of the saddle point  $\delta\nu \sim 1/(a\Delta Y)^2 \sim 0.3$  (for  $\alpha_s = 0.3$ ) becomes sufficiently small. Thus, if we choose  $Y_M = \Delta Y = Y - Y_M = 4$ ,  $\alpha_s = 0.3$  and  $\mathbf{l} = 1 \text{ GeV}^{-1}$ , we obtain  $g_{3P} \sim 0.6 \text{ GeV}^{-1}$ . It follows from (59) and from our discussion before that this value has large theoretical uncertainties: changes in  $\mathbf{l}$ ,  $Y$  and  $Y_M$  have a stronger influence on the numerical value of the perturbative triple Pomeron vertex than on the nonperturbative triple Pomeron coupling. As the result of our analysis, we therefore present the range

$$g_{3P} \sim 0.2 - 1.7 \text{ GeV}^{-1} \quad (64)$$

which is related to the ranges of values  $3 < \Delta Y < 5$  and  $0.5 \text{ GeV}^{-1} < \mathbf{l} < 2 \text{ GeV}^{-1}$ . Surprisingly, these numerical value are not far from the experimental value discussed before.

Finally, we would like to mention that this perturbative value may be a little overestimated. Namely, we have to remember that, in order to arrive at the triple Regge cross section formula, we had to take the discontinuity of  $a_6$  at  $\mathbf{l}_\alpha = 0$ . In analogy with the impact factor (18), the triple Pomeron vertex at  $\mathbf{l}_\alpha$  has a singularity  $\sim 1/\nu$  just at the saddle point  $\nu = 0$ ; as we have discussed in section 2, this singularity is a result of the massless gluon

---

<sup>5</sup>In particular, the gap survival probability within the ISR energy domain, calculated in the formalism of ref. [23], is equal to  $S^2 = 0.25 - 0.33$ .

propagator, and it should disappear after the introduction of an appropriate infrared cutoff. Numerically, the presence of the  $1/\nu$  singularity should lead to enhancement, and our value of the perturbative triple Pomeron vertex may, in fact, therefore be overestimated.

It is interesting to compare our result with the numerical studies of the Balitsky-Kovchegov equation [9, 24, 25] (BK) equation. The equation includes the LO BFKL evolution and accounts for the triple Pomeron coupling summing up the fan diagrams in terms of the dipole-dipole interaction. In the recent paper [26] the beginning of saturation was observed at rather small  $Y \sim 2 - 3$ . However first the saturation is reached for a large size dipole where the absorptive corrections are much stronger. This is a dangerous region. Even without the confinement and for a fixed  $\alpha_s$  coupling we faced here two problems:

on one hand, at small  $l$  ( $k$  in the notations of [26]) the  $1/\nu$  singularity plays a crucial role, as it was discussed above,

on other hand, the whole approach can be justified only for the case when the rapidity interval  $\Delta Y$  occupied by each Pomeron is large enough. there is no this condition in BK-equation and the Pomerons can split immediately, especially for a large size dipoles.

To avoid these problems we focus on dipoles of a smaller size, smaller than the initial (input) size  $1/k_0$ , taken in [26] to be  $1 \text{ GeV}^{-1}$ . Here the absorptive effects reveal itself at  $Y \sim 4 - 6$  (see Fig.2,4 of ref.[26]). This is in agreement with our expectation. Based on the simplified form of the first (order of  $g_{3P}$ ) fan diagram contribution (23,24) and taken the effective perturbative vertex  $g_{3P} \sim 0.6 \text{ GeV}^{-1}$  (which was evaluated just for  $\Delta Y \sim 4$ ), we found that the triple Pomeron amplitude becomes comparable with the single Pomeron exchange at  $Y \sim 4 - 5$ ; we choose  $l \sim 1 \text{ GeV}$ ,  $g_N = 10 \text{ GeV}^{-1}$  (corresponding to  $\sigma_{pp}^{tot} = 40 \text{ mb}$  and  $\alpha_s = 0.2$  (corresponding to the LO BFKL  $\omega_0 = 0.56$ ) as it was done in [26]).

## 5.2 Renormalization of the Pomeron intercept due to the Pomeron selfenergy

Finally, we estimate the size of the Pomeron self energy correction and its influence on the intercept of the perturbative BFKL amplitude. In the loop amplitude (62) we still have the integrals over the rapidities  $Y_1, Y_2$ , and the dominant contribution comes from the region of small  $Y_1, Y_2$ , where  $\Delta Y = |Y - Y_1 - Y_2| \rightarrow Y$ . This limit corresponds to a two-Pomeron exchange of eikonal type. On the other hand, (62) was derived under the assumption that  $Y_1$  and  $Y_2$  are large enough to justify the insertion of BFKL Pomerons between the loop and the impact factors, and we have to restrict  $\Delta Y$  to a region smaller than the total rapidity. If the total rapidity  $Y$  is much larger than the rapidity interval occupied by the loop - for example we could consider a loop of the finite size  $\Delta Y$  with  $\Delta Y \sim 1/\omega_0 \sim 4$  - then such a "small" loops can be repeated many times and would play the role of the Pomeron self energy, leading to a renormalization of the Pomeron intercept. As mentioned before, the self energy is negative relative to the BFKL amplitude, and the renormalization therefore lowers the Pomeron intercept. If the absolute value of the renormalization is close or even larger than the 'bare' intercept  $\omega_0 = \alpha(0) - 1$ , one may get close to the "critical" Pomeron or even obtain the "subcritical" Pomeron, as it has been discussed in [3, 4, 27] (see also [28] where a prescription for the renormalization of the supercritical (with  $\alpha(0)_P > 1$ ) Pomeron was

proposed).

Before we do our estimate, it is useful to recall the nonperturbative renormalization caused by the pion loop insertion. For a single pion loop inside the Pomeron (at  $t = 0$ ) we have a formula quite analogous to (62). Instead of  $Y_1, Y_2$ , convenient variables are: the size of the loop  $\Delta Y$ , the position of the center of the loop  $Y_c = (Y - Y_1 + Y_2)/2$ . Inside the pion loop we have the transverse momentum  $k_t$  of the pion. Let us fix, for a moment, the value of  $Y_c$  and calculate the pion loop contribution  $\Delta^\pi$ :

$$\Delta^\pi = \frac{3g_\pi^2}{16\pi^3} \int d(\Delta Y) dk_t^2 \frac{[k_0^2 e^{-\Delta Y}]^2}{[k_t^2 + m_\pi^2 + k_0^2 e^{-\Delta Y}]^2} \approx \frac{3g_\pi^2 k_0^2}{16\pi^3} \int d(\Delta Y) e^{-\Delta Y} \sim 0.1. \quad (65)$$

Here the first factor 3 results from the contributions of  $\pi^+$ ,  $\pi^0$  and  $\pi^-$ . For the numerical estimate we neglect the pion mass  $m_\pi$ , put the Pomeron pion coupling square  $g_\pi^2 = \sigma_{\pi\pi}(s_0) \sim 20$  mb and choose the mean transverse momentum of the first particle inside the Pomeron-pion vertex  $k_0 \sim 0.6$  GeV. One needs this particle also to fix the rapidity of the vertex  $Y_1$  (or  $Y_2$ ). The integral over  $\Delta Y$  (65) is convergent, and for  $\Delta Y \ll Y$  the integration over  $Y_c$  gives a factor  $Y$ . As a result, the one loop correction to the amplitude is equal to  $Y \cdot \Delta^\pi$ . Inserting two pion loops we obtain  $\frac{1}{2}(Y \cdot \Delta^\pi)^2$ , and summing over an arbitrary of loops we get the sum  $\exp(Y \cdot \Delta^\pi)$  which means that the Pomeron intercept increases by  $\Delta^\pi$ .

Returning to the perturbative Pomeron loop insertion (62), we again choose  $\alpha_s = 0.3$  and assume  $Y \gg \Delta Y$ . Dividing the amplitude (62) by the elastic forward amplitude (20) and considering only the integration over the loop size, we find:

$$\Delta^{loop} = \int \frac{2\pi e^{x_0 \Delta Y}}{[a \Delta Y]^3} \frac{C_{4V}^2}{(4\pi)^{17}} d(\Delta Y) \approx 2.53 \cdot 10^{-3} \frac{\delta Y}{[\Delta Y]^3} e^{\omega_0 \Delta Y}. \quad (66)$$

Here we have cut the integration over the loop size at  $\delta Y = \Delta Y$ . As the numerical coefficient here is extremely small, the only possibility to obtain a relatively large renormalization is to chose a very large  $\Delta Y \gg 1/\omega_0$ . On the other hand the loop renormalization  $\Delta^{loop}$  is a NNLO BFKL effect and first we have to account for the NLO BFKL corrections which lowers the intercept down to  $\omega_0 \sim 1/4$ . Therefore up to a very large  $\Delta Y$  the loop renormalization is still negligible; for  $\omega_0 = 0.25$  the values of  $\Delta^{loop}$  and  $\omega_0$  become comparable only for  $\Delta Y > 45$  (changing the value of  $\omega_0$  to the larger value  $\omega_0 = 0.70$  we are consistent with [15, 20]). Of course, from the academic point of view we have to account for this renormalization effect, when  $s \rightarrow \infty$ ; but at any reachable rapidity interval the value of  $\Delta^{loop}$  is much less than  $\omega_0$ .

Since the numerical value of the triple Pomeron coupling is not far from the nonperturbative one, it is not surprising to see that the estimate (66) is also consistent with the nonperturbative evaluation. In the latter case we expect

$$\Delta_{n.p.}^{loop} \sim \frac{g_{3P}^2}{16\pi^3} \int d(\Delta Y) dk_t^2 e^{\omega_0 \Delta Y} \approx 2 \cdot 10^{-3} \delta Y e^{\omega_0 \Delta Y} \quad (67)$$

for  $g_{3P} \sim 1$  GeV<sup>-1</sup> and  $k_t^2 \sim 1$  GeV<sup>2</sup>.

Finally we mention that the estimate in (66) may still be a bit too large. Namely, recall that in our calculation of the Pomeron self energy and in our numerical estimate of its

magnitude we have restricted ourselves to the forward direction, that we have considered the values  $\mathbf{l}_\alpha = \mathbf{l}'_\alpha = 0$ . As discussed before, this is the point where the perturbative nature of the BFKL approximation becomes most visible, i.e. the 'distance' between pQCD and nonperturbative QCD is the largest. The mathematical manifestation is the  $1/\nu$  singularity, which immediately disappears if we depart from  $\mathbf{l}_\alpha = 0$ . Therefore, as for the discussion of the numerical value of the triple Pomeron coupling, we expect that also our estimate of the renormalization due to the selfenergy may be slightly overestimated.

## 6 Conclusions

In this paper we have performed an estimate of the perturbative triple Pomeron vertex. Starting from the results of a leading- $\ln s$  analysis of QCD perturbation theory in the triple Regge limit, we have used the large- $N_c$  limit to derive a fairly simple expression for the triple Regge inclusive cross section, which can be compared with the standard formulae used in the analysis of experimental data. A numerical estimate of the perturbative triple Pomeron coupling - which has a considerable theoretical uncertainty - indicates that its value is of the same order of magnitude as the nonperturbative one, obtained from earlier fits to experimental data.

We have also tried to estimate the renormalization of the BFKL intercept due the Pomeron self energy loop. Formally speaking, this is NNLO effect and lies beyond the NLO corrections to the BFKL kernel. A numerical estimate - again with theoretical uncertainties - indicates that these corrections due to self interactions of the BFKL Pomeron are much smaller than the nonperturbative contribution (65). This is caused by the fact that this correction is proportional to the perturbative triple Pomeron vertex square, and it agrees with the evaluation of the Pomeron loop insertion based on the phenomenological value (63) of the triple Pomeron vertex..

So finally we conclude that in spite of a 'huge number'  $\Omega = 7767$  (see eq.(54)) the perturbative triple Pomeron coupling is not large; it is in approximate agreement with the old phenomenological evaluations.

As a future step, it would be interesting to understand better why numerical studies of the nonlinear evolution equations seem to find rather rapid saturation effects in spite of a rather small value of the perturbative triple Pomeron coupling.

## Appendix A: Counting factors of 2 and $\pi$

In this appendix we give a brief summary of the normalization of the impact factors and the triple Pomeron vertex in perturbative QCD. Our starting point is eq.(4) which defines the impact factor. To be definite we consider the elastic scattering of two quarks (averaged over color and helicity of the incoming quarks). The lowest order diagram with color singlet exchange has two gluons in the t-channel (box diagram and its crossed counterpart), and in

the high energy limit on finds

$$A_{el}^{LO} = isg^4 \frac{N_c^2 - 1}{(2N_c)^2} \int \frac{d^2 \mathbf{k}}{(2\pi)^2} \frac{1}{\mathbf{k}^2 (\mathbf{q} - \mathbf{k})^2}. \quad (68)$$

Comparison with (4) yields the quark impact factor

$$\Phi_q = 2\sqrt{\pi}g^2 \frac{\sqrt{N_c^2 - 1}}{2N_c}. \quad (69)$$

Equivalently, we could have defined the impact factor through the requirement that the leading order energy discontinuity should have the form

$$disc A_{el} = \int \frac{d^2 \mathbf{k}}{(2\pi)^3} \Phi_q \frac{1}{\mathbf{k}^2 (\mathbf{q} - \mathbf{k})^2} \Phi_q. \quad (70)$$

Next we turn to the triple Regge cross section. Eq.(23) defines the  $M^2$ -discontinuity of a six-point function,  $a_6$ . Turning again to lowest order QCD diagrams, we look at the diffractive process  $q + q \rightarrow (qg) + qa$  in the triple Regge limit; a typical QCD diagram is shown in Fig.5. We define the triple Pomeron vertex through the LO equation

$$a_6 = 2s \int \frac{d^2 \mathbf{q}}{(2\pi)^3} \frac{d^2 \mathbf{k}_1}{(2\pi)^3} \frac{d^2 \mathbf{k}_3}{(2\pi)^3} \Phi_q \frac{1}{(\mathbf{q}^2)^2} V(\mathbf{q}, -\mathbf{q} | \mathbf{k}_1, \mathbf{l} - \mathbf{k}_1; \mathbf{k}_3, \mathbf{l} - \mathbf{k}_3) \frac{1}{\mathbf{k}_1^2 (\mathbf{l} - \mathbf{k}_1)^2} \Phi_q \frac{1}{\mathbf{k}_3^2 (\mathbf{l} + \mathbf{k}_3)^2} \Phi_q. \quad (71)$$

The analysis of the high energy behavior of the relevant QCD diagrams leads to the result:

$$4a_6 = \pi^3 \frac{N_c^2 - 1}{2N_c} g^{10} \int \frac{d^2 \mathbf{q}}{(2\pi)^3} \frac{1}{(\mathbf{q}^2)^2} \tilde{V}(\mathbf{q}, -\mathbf{q} | \mathbf{k}, \mathbf{l} - \mathbf{k}; \mathbf{k}, \mathbf{l} - \mathbf{k}) \frac{1}{\mathbf{k}_1^2 (\mathbf{l} - \mathbf{k}_1)^2} \frac{1}{\mathbf{k}_3^2 (\mathbf{l} + \mathbf{k}_3)^2} \quad (72)$$

where  $\tilde{V}$  stands for the BFKL-type  $2 \rightarrow 4$  gluon vertex:

$$\tilde{V} = \frac{(\mathbf{q}^2)^2}{(\mathbf{q} - \mathbf{k}_1)^2 (\mathbf{l} + \mathbf{k}_3 - \mathbf{q})^2} - \frac{\mathbf{q}^2}{(\mathbf{q} - \mathbf{k}_1)^2 \mathbf{k}_1^2} - \frac{\mathbf{q}^2}{(\mathbf{l} + \mathbf{k}_3)^2 (\mathbf{l} + \mathbf{k}_3 - \mathbf{q})^2} \quad (73)$$

Inserting the result for the quark impact factor we obtain the following normalization of the triple Pomeron vertex  $V$ :

$$V = \frac{(2N_c)^2 g^4 \pi^{3/2}}{\sqrt{N_c^2 - 1} 32} \tilde{V} \quad (74)$$

## Appendix B: Impact factors in the conformal approximation

We discuss here briefly, with simple arguments and some approximations, the behaviour of the impact factors in conformal representation in the forward and non forward direction, but without giving a full momentum and conformal weight dependence.

Let us consider already the situation of zero conformal spin and work in coordinate representation. One can obtain the same results on studying the limiting case of the BFKL Pomeron eigenstate in momentum representation.

We start from an impact factor which have some dominant support in a bounded region of size of order  $R$  in the coordinate space. We are interested in studying the behaviour of the following expression

$$\Phi(\nu, \mathbf{l}) = \int \frac{d^2 \mathbf{r}_1}{(2\pi)^2} \frac{d^2 \mathbf{r}_2}{(2\pi)^2} |r_{12}|^{1+2i\nu} \Phi(\mathbf{r}_1, \mathbf{r}_2) \int \frac{d^2 \mathbf{r}_0}{(2\pi)^2} e^{i\mathbf{r}_0 \mathbf{l}} (|r_{10}| |r_{20}|)^{-1-2i\nu}. \quad (75)$$

We are mainly interested in studying the behaviour in the small  $|\mathbf{l}|$  region. Therefore the main contribution in (75) will come from the integration in the region of large  $|\mathbf{r}_0|$ . It is therefore convenient to split the integration region according to  $|\mathbf{r}_0| < R$  and  $|\mathbf{r}_0| > R$ . We shall be interested therefore in momenta  $|\mathbf{l}| < 1/R$  and neglect the first contribution. We note also that in the region  $|\mathbf{r}_0| > R$  it is a good approximation to consider  $|r_{i0}| \approx |\mathbf{r}_0|$  for  $i = 1, 2$  since the external integral has support roughly for  $|r_i| < R/2$ . We can therefore write, in a factorized form,

$$\Phi(\nu, \mathbf{l}) \approx \int \frac{d^2 \mathbf{r}_1}{(2\pi)^2} \frac{d^2 \mathbf{r}_2}{(2\pi)^2} |r_{12}|^{1+2i\nu} \Phi(\mathbf{r}_1, \mathbf{r}_2) \int_{|\mathbf{r}_0| > R} \frac{d^2 \mathbf{r}_0}{(2\pi)^2} e^{i\mathbf{r}_0 \mathbf{l}} (|r_0|^2)^{-1-2i\nu} = \phi_\nu g(\nu, \mathbf{l}) \quad (76)$$

and study the  $\mathbf{l}$  dependence in  $g(\nu, \mathbf{l})$ . The  $\mathbf{r}_0$  integration gives

$$\begin{aligned} g(\nu, \mathbf{l}) &= \pi R^{-4i\nu} \frac{1}{2i\nu} \left( {}_1F_2(-2i\nu, 1, 1 - 2i\nu; -\frac{R^2 \mathbf{l}^2}{4}) - \frac{\Gamma(1 - 2i\nu)}{\Gamma(1 + 2i\nu)} \left(\frac{R^2 \mathbf{l}^2}{4}\right)^{2i\nu} \right) \\ &= \pi R^{-4i\nu} \left\{ \frac{1}{2i\nu} \left[ 1 - \left(\frac{R^2 \mathbf{l}^2}{4}\right)^{2i\nu} \right] + \frac{R^2 \mathbf{l}^2}{4} \right\} + O(\nu) + O\left(\left(\frac{R^2 \mathbf{l}^2}{4}\right)^2\right) \end{aligned} \quad (77)$$

One can see that in the forward direction  $\mathbf{l} = \mathbf{0}$  the second term does not give contribution and therefore  $g(\nu, \mathbf{l}) \sim 1/(2i\nu)$ . This leads infact to the correct behaviour of the BFKL Pomeron Green's function in forward direction, where under the  $\nu$  integration the integrand is not proportional to  $\nu^2$ , as, instead, in the non forward case. To analyze the limit of small  $\mathbf{l} R^2 \rightarrow \mathbf{0}$  one can keep the term  $(R^2 \mathbf{l}^2)^{2i\nu}/(2i\nu)$  and estimate with the saddle point method its contribution in such a limit. Again one can easily check that such a contribution is suppressed. For  $\mathbf{l} \neq \mathbf{0}$  there is instead a cancellation of the  $\nu$  pole in the origin. Therefore we can write

$$\begin{aligned} \Phi(\nu, \mathbf{0}) &\approx \frac{1}{i\nu} \Phi_{0F} \\ \Phi(\nu, \mathbf{l}) &\approx \Phi_{0NF}, \quad s \gg \mathbf{l}^2 > 0 \end{aligned} \quad (78)$$

We shall be interested typically, for the non forward case, to values of  $R|\mathbf{l}| \sim 1$ , at the border of the approximations taken above to show the behaviour in (78).

## References

- [1] E. A. Kuraev, L. N. Lipatov and V. S. Fadin, Sov. JETP **44** (1976) 443; ibid. **45** (1977) 199; Ya. Ya. Balitskii and L.N. Lipatov, Sov. J. Nucl. Phys. **28**, (1978) 822.
- [2] V. S. Fadin and L. N. Lipatov, Phys. Lett **B429** (1998) 127, and references therein; M. Ciafaloni and G. Camici, Phys. Lett. **B430** (1998) 430.
- [3] A.A.Migdal, A.M. Polyakov, K.A. Ter-Martirosyan, Phys.Lett.**B48** (1974) 239.
- [4] H.D.I.Abarbanel and J.B.Bronzan, Phys.Lett.**B48** (1974) 345; Phys.Rev **D9** (1974) 2397; H.D.I.Abarbanel, J.B.Bronazan, R.L.Sugar, and A.R.White, Phys.Rep.**21C** (1975) 119.
- [5] J. Bartels, Phys.Lett. B 298 (1993) 204; Z. Phys. **C60** (1993) 471.
- [6] J. Bartels and M. Wüsthoff, Z. Phys. **C66** (1995) 157.
- [7] M.Braun, Z.Phys.**C71** (1996) 123; M.Braun and G.P.Vacca, Eur.Phys.J.**C6**, 147 (1999); M.Braun, Eur.Phys.J.**C6** 321 (1999);
- [8] G. P. Vacca, “The hard QCD pomeron: Some aspects of its phenomenology and interactions”, arXiv:hep-ph/9803283
- [9] I.I.Balitsky, Nucl.Phys.**B463**, 99 (1996)
- [10] A.H.Mueller and B.Patel, Nucl.Phys.**B425** 471 (1994)
- [11] R.Peschanski, Phys.Lett.B 409, 491 (1997).
- [12] A.Bialas, H.Navelet, and R.Peschanski, Phys.Lett.**B427** (1998) 147; Phys.Rev.**D57**, R6585 (1998)
- [13] G.P. Korchemsky, Nucl.Phys.B550:397-423,1999 and e-Print Archive: hep-ph/9711277.
- [14] M.Braun, Phys.Lett.**B425** (1998) 354.
- [15] A.H. Mueller and G.P. Salam, Nucl.Phys.**B475**:293-320,1996. e-Print Archive: hep-ph/9605302
- [16] J. Bartels, M. A. Braun, D. Colferai and G. P. Vacca, Eur.Phys.J.C **20** (2001) 323 [arXiv:hep-ph/0102221].
- [17] L.N. Lipatov, *Pomeron in quantum chromodynamics*, in “Perturbative QCD”, pp. 411-489, ed. A. H. Mueller, World Scientific, Singapore, 1989; Phys. Rep. **286** (1997) 131.
- [18] J.C.Collins, P.V.Landshoff, Phys.Lett. **B276** (1992) 196

- [19] M.F.McDermott, J.R.Forshaw, Nucl.Phys. **B484** (1997) 283.
- [20] G.P.Salam, Nucl.Phys.**B461**:512-538,1996. e-Print Archive: hep-ph/9509353
- [21] A.B.Kaidalov, V.A.Khoze, Yu.F.Pirogov, N.L.Ter-Isakyan, JETP Letters **17** (1973) 626; A.B.Kaidalov, V.A.Khoze, Yu.F.Pirogov, N.L.Ter-Isakyan, Phys.Letters **B45** (1973) 493.
- [22] R.D.Field, C.C.Fox, Nucl.Phys. **B80** (1974) 367
- [23] V.A.Khoze, A.D.Martin, M.G.Ryskin, Eur.Phys.J. **C18** (2000) 167.
- [24] I.I.Balitsky, Phys.Rev.Lett. **81** (1998) 2024; Phys.Rev. **D60** (1999) 014020; Phys.Lett. **B518** (2001) 235.
- [25] Yu.V.Kovchegov, Phys.Rev. **D60** (1999) 034008.
- [26] K.Golec-Biernat, L.Motika, A.M.Stasto, Phys.Rev. **D65** (2002) 074037.
- [27] A.B.Kaidalov, Phys.Rep.**50** (1979) 157.
- [28] A.B,Kaidalov, L.A.Ponomarev, K.A.Ter-Martirosyan, Sov.Jour.Nucl.Phys. **44** (1986) 468